Bulletin of Electrical Engineering and Informatics
Vol. 14, No. 6, December 2025, pp. 4495~4506
ISSN: 2302-9285, DOI: 10.11591/eei.v14i6.10250

New perspective in enhancing Papanicolaou-smear image using CLAHE and spider monkey optimization

Ach Khozaimi[1,3], Wuryansari Muharini Kusumawinahyu[1], Isnani Darti[1], Syaiful Anam[1], Ulfatun Nahdhiyah[2]
[1]Department of Mathematics, Faculty of Mathematics and Natural Sciences, Brawijaya University, Malang, Indonesia
[2]Department of Pathology Anatomy, Faculty of Medicine, Brawijaya University, Malang, Indonesia
[3]Department of Informatics Engineering, Faculty of Engineering, University of Trunojoyo Madura, Bangkalan, Indonesia

Article Info

Article history:

Received Mar 11, 2025
Revised Oct 3, 2025
Accepted Oct 20, 2025

Keywords:

Cervical cytology
Contrast enhancement-based image quality
Contrast-limited adaptive histogram equalization
Image enhancement
Pap smear
Spider monkey optimization

ABSTRACT

High-quality Papanicolaou (Pap) smear images are essential for reliable early detection of cervical cancer, yet low contrast and noise often hinder accurate interpretation. This study introduces spider monkey optimization (SMO)-contrast-limited adaptive histogram equalization (CLAHE), an optimized CLAHE framework guided by the SMO algorithm. A novel signal contrast (SC) objective function is proposed, combining perceptual enhancement contrast enhancement-based image quality (CEIQ) with fidelity preservation peak signal-to-noise ratio (PSNR) to adaptively tune CLAHE parameters. Experiments on the publicly available SIPaKMeD and Mendeley LBC datasets demonstrate that SMO-CLAHE consistently outperforms manual settings and flower pollination algorithm (FPA)-based optimization, and achieves performance comparable to pelican optimization algorithm (POA) across key quality metrics including entropy, structural similarity index (SSIM), PSNR, enhancement measure estimation (EME), root mean square contrast (RMSC), standard deviation (STD-DEV), and CEIQ. Furthermore, downstream evaluation using a MobileNetV3-S classifier shows that the enhanced images lead to improved cervical cancer classification performance. These results highlight SMO-CLAHE as a robust and clinically relevant preprocessing framework, offering a new perspective for Pap smear image enhancement and diagnostic support.

Corresponding Author:

Wuryansari Muharini Kusumawinahyu
Department of Mathematics, Faculty of Mathematics and Natural Sciences, Brawijaya University
Malang, East Java, Indonesia
Email: wmuharini@ub.ac.id

1. INTRODUCTION

Cervical cancer is still a leading cause of female cancer mortality worldwide, especially in low- and middle-income regions lacking early screening [1], [2]. The Papanicolaou (Pap) smear test is a standard early detection method, but its accuracy depends on the quality of the images [3]. In practice, Pap smear images often suffer from low contrast and imaging noise caused by variations in staining, illumination, and acquisition devices, making it difficult for cytologists to identify subtle morphological features [4].

To mitigate these limitations, contrast enhancement is commonly applied as a preprocessing step in medical image analysis [5]. Histogram equalization (HE) and its local variant, adaptive histogram equalization (AHE), are classical methods [6], but AHE can cause excessive enhancement and increase noise in uniform regions. Contrast-limited adaptive histogram equalization (CLAHE) addresses this issue by introducing a clip limit to control contrast amplification [7]. CLAHE has been successfully applied in diverse

tasks, including cervical cancer classification [8], object detection in low-light conditions [9], deep learning-based medical image analysis [10], and segmentation of CT and underwater images [11], [12]. However, the performance of CLAHE depends strongly on two parameters—clip limit and tile grid size. Fixed parameter settings, such as the configuration proposed by Qassim *et al.* [13] (clip limit=0.01, tile size=8×8), may work for specific datasets but often fail to generalize across imaging conditions.

To overcome this sensitivity, many studies have employed metaheuristic optimization to automate the selection of CLAHE parameters. Multi-objective particle swarm optimization (MOPSO) [14], whale optimization algorithm (WOA) [15], cuckoo search algorithm (CSA) [16], flower pollination algorithm (FPA) [17], adaptive sailfish optimization (ASFO) [18], cat swarm optimization (CSO) [19], and the pelican optimization algorithm (POA) [20] have all shown improvements when evaluated with metrics such as entropy, structural similarity index (SSIM), peak signal-to-noise ratio (PSNR), and standard deviation (STD-DEV). Although effective, these methods still leave room for alternative optimizers with stronger global search capability, higher efficiency, and more robust convergence.

Spider monkey optimization (SMO) is a relatively recent swarm-intelligence algorithm inspired by the fission–fusion foraging behavior of spider monkeys. Its adaptive leader–follower mechanism has proven effective for complex optimization tasks [21], [22]. Building on these strengths, this study introduces a new framework, SMO-CLAHE, to adaptively determine the optimal clip limit and tile grid size for enhancing Pap smear images. A key innovation is the use of signal contrast (SC) as the optimization objective SC combines contrast enhancement-based image quality (CEIQ) with PSNR through a multiplicative formulation, encouraging simultaneous improvement of perceptual contrast and noise suppression. CEIQ itself integrates cross-entropy, entropy, and SSIM to evaluate enhancement quality while preserving structural fidelity [23], [24]. Including PSNR ensures that contrast improvements do not come at the cost of excessive noise.

The main contribution of this work is the development of a novel SMO-CLAHE framework that introduces SC as a new optimization goal to balance contrast enhancement and structural preservation. Unlike previous methods that rely solely on traditional metrics or fixed parameter choices, the proposed approach jointly optimizes CLAHE parameters using a metaheuristic search to improve both perceptual quality and noise control. The framework is thoroughly evaluated on SIPaKMeD and Mendeley LBC datasets using a broad range of image quality metrics—including entropy, SSIM, PSNR, enhancement measure estimation (EME), root mean square contrast (RMSC), STD-DEV, and CEIQ. It is further validated through a downstream classification task with a MobileNetV3-S model to demonstrate its practical value in cervical cancer detection. By combining an effective metaheuristic search strategy with a clinically relevant image quality metric, this study advances automated preprocessing for cervical cancer screening beyond basic parameter tuning, providing empirical evidence of its benefits for real diagnostic applications.

2. METHOD

2.1. Image contrast enhancement

Image contrast enhancement is a method that amplifies the brightness difference between objects and backgrounds, making objects more noticeable [25]. HE, AHE, and CLAHE are widely used for enhancing image contrast, including in medical images. HE redistributes pixel intensities to produce a uniform histogram [26]. The probability $P(r_i)$ of each intensity i is (1):

$$P(r_i) = \frac{n_i}{N} \tag{1}$$

where n_i is the number of pixels with intensity i and N is the total number of pixels. The cumulative distribution function (CDF) is (2):

$$CDF(r_i) = \sum_{j=0}^{i} P(r_i) \tag{2}$$

and the new intensity is (3):

$$i_{new} = round\left(CDF(r_i) \times (L-1)\right) \tag{3}$$

with L as the number of intensity levels (e.g., 256). HE works well globally but can create artefacts with skewed histograms. AHE applies HE to smaller image regions (tiles) to improve local contrast [26]:

$$i_{new}(p) = round\left(CDF_{tile}(r_i) \times (L-1)\right) \tag{4}$$

where $CDF_{\text{tile}}(i)$ is the CDF within a tile. AHE handles uneven lighting but may amplify noise in uniform areas. CLAHE prevents over-enhancement by limiting the histogram count with a clip limit β [27]:

$$\widehat{h_t}(i) = min(h_t(i), \beta), E_t = \sum_{i=0}^{L-1} max\,(0,\, h_t(i) - \beta) \quad (5)$$

$$\widetilde{h_t}(i) = \widehat{h_t}(i) + \frac{E_t}{L}, s_k^{(t)} = (L-1)\,\widetilde{T_t}(r_k) \quad (6)$$

where $\widetilde{T_t}$ is the CDF of $\widetilde{h_t}$. Neighboring tiles are blended by bilinear interpolation. The CLAHE has two parameters that can be fine-tuned to optimize its performance. Each technique has its strengths and weaknesses. HE is computationally efficient and suitable for global enhancement, whereas AHE and CLAHE are better for localized contrast improvement, with CLAHE being the most noise-robust [28].

2.2. Spider monkey optimization

The foraging and social behavior exhibited by spider monkeys serves as a model for the development of the SMO algorithm. The goal is to find the best solution for complex optimization problems by copying the collaborating and adaptable behaviors of spider monkeys [21]. In SMO, each candidate (monkey) $SM_k = [SM_{k1}, \ldots, SM_{kD}]$ in $D - dimensional$ space is initialized using by (7):

$$SM_{kj} = SM_{min\,j} + R\left(SM_{max\,j} - SM_{min\,j}\right) \quad (7)$$

Local leader (LL) update: each monkey updates its position based on its local leader $Leader_{kj}$, and a random peer SM_{rj}:

$$SM_{ij}^{new} = SM_{ij} + R\left(Leader_{kj} - SM_{ij}\right) + U\left(SM_{rj} - SM_{ij}\right) \quad (8)$$

Global leader (GL) selection: the probability of a solution being updated using (9):

$$prob_i = 0.9 \times \frac{fitness_i}{max_{fitness}} + 0.1 \quad (9)$$

where R and U are uniformly sampled from $[0,1]$ and $[-1,1]$, respectively; after each update, we clamp SM_{ij} to its bounds to prevent invalid parameters:

$$SM_{ij} = min\left(max\left(SM_{ij}, SM_{min\,j}\right), SM_{max\,j}\right) \quad (10)$$

The best solution becomes the global leader, while subgroup leaders act as local leaders. Suppose no progress is made for a set number of steps. In that case, the local leader decision (LLD) reinitializes solutions, and the global leader decision (GLD) splits or merges groups to encourage exploration. SMO has been successfully used to optimize neural networks for intrusion detection systems and solve complex problems like optimizing redundant units for CoRAP in water treatment plants [29], [30].

2.3. Contrast enhancement-based image quality

The CEIQ method is designed to evaluate the quality of an image by analyzing how effectively its contrast has been improved. The procedure, as illustrated in Figure 1, begins with decolorization, where the original color image is converted into a grayscale version to simplify intensity-based analysis. Next, HE is applied to the grayscale image, enhancing its contrast by redistributing pixel intensities across the available range. Both the original and enhanced grayscale images undergo histogram computation, which generates intensity distributions for further evaluation.

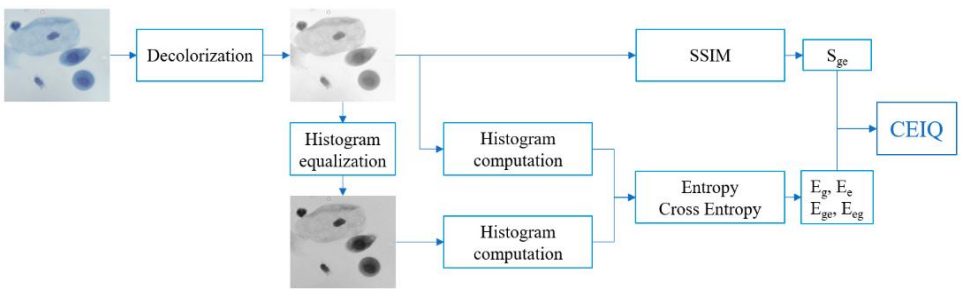

Figure 1. CEIQ evaluation model

The quality assessment is based on three main components:

a. Image similarity: this step measures how closely the enhanced image retains the structural content of the original image. The SSIM is used for this purpose, producing a similarity score S_{sc} that reflects luminance, contrast, and structural preservation. SSIM is defined as (11):

$$SSIM(I,\hat{I}) = \frac{(2\mu_I\mu_{\hat{I}}+C_1)(2\sigma_{I\hat{I}}+C_2)}{(\mu_I^2+\mu_{\hat{I}}^2+C_1)(\sigma_I^2+\sigma_{\hat{I}}^2+C_2)} \quad (11)$$

where $\mu_I, \mu_{\hat{I}}$ are mean intensity of I and $\hat{I}$, $\sigma_I^2, \sigma_{\hat{I}}^2$ is variance of I and $\hat{I}$. $\sigma_{\hat{I}}, \sigma_I$ are covariance between I and $\hat{I}$. C_1, C_2 are small constants to stabilize the division.

b. Entropy: this measures the amount of information or detail in the image by evaluating how uniformly brightness values are distributed. A higher entropy value generally indicates richer image details and improved contrast.

$$\text{Entropy} = -\sum_{i=0}^{L-1} p_i \, log_2(p_i) \quad (12)$$

where p_i is the probability of occurrence of the intensity level i. Higher entropy values suggest more detailed and complex images, while lower values imply a uniform or less informative image.

c. Cross-entropy: this quantifies the difference between the intensity histograms of the original and enhanced images. It is computed as (13):

$$E_{x,y} = -\sum_{i=0}^{b} h_x(i) \log\left(h_y(i)\right) \quad (13)$$

where $h_x(i)$ and $h_y(i)$ represent the normalized histogram values of the enhanced and original images, respectively, b is the total number of histogram bins. The CEIQ score is computed by combining the SSIM, entropy, and cross-entropy metrics. This composite score reflects both the preservation of structural similarity and the enhancement of image contrast, making it a robust measure for evaluating contrast enhancement quality [31].

2.4. Image quality assessment

IQA is used to evaluate the quality of digital images. There are three main types of IQA models: no-reference image quality assessment (NR-IQA), reduced-reference image quality assessment (RR-IQA), and full-reference image quality assessment (FR-IQA) [32]. In this study, several IQA metrics were used to evaluate the effectiveness of the proposed image enhancement method [33].

– EME is defined as (14):

$$\text{EME} = \frac{1}{M\times N}\sum_{i=1}^{M}\sum_{j=1}^{N}\left[20\, log\left(\frac{I_{max}(i,j)}{I_{min}(i,j)}\right)\right] \quad (14)$$

where M and N are the image height and width. $I_{\min}(i,j)$ and $I_{\max}(i,j)$ are the minimum and maximum pixel intensities in a block at position (i,j). Higher EME values indicate better local contrast and sharper details in the image.

– RMSC quantifies the overall contrast of the image by calculating the deviation of each pixel's intensity from the average intensity $\bar{I}$. It is calculated as (15):

$$\text{RMSC} = \sqrt{\frac{1}{M\times N}\sum_{i=1}^{M}\sum_{j=1}^{N}(I(i,j)-\bar{I})^2} \quad (15)$$

where $I(i,j)$ represents the intensity of the pixel at (i,j) position, and $\bar{I}$ is the average intensity of all pixels. A higher RMSC reflects more distinct separation between features in the image.

– Standard deviation (STD-DEV) measures the variation in pixel intensities, calculated as (16):

$$\text{STD DEV} = \sqrt{\frac{1}{N}\sum_{i=1}^{N}(I_i-\mu)^2} \quad (16)$$

where I_i is the intensity of pixel i, and μ is the mean intensity of the image. A higher standard deviation indicates greater contrast and image variation, contributing to improved image clarity and detail preservation.

2.5. Experimental setup

Figure 2 illustrates the workflow of the proposed CLAHE optimization using SMO. We used the SIPaKMeD dataset (five cervical cell classes) [34]. RGB images were converted to CIELAB; the L channel (luminance) was enhanced while preserving a/b (chromaticity) [35]. SMO optimized clip limit and tile grid size with 30 iterations and population size 50 [16]. The search ranges for the clip Limit were from 0.01 to 3, and for the tile grid size, from 2×2 to 16×16. These ranges were selected to incorporate the widely used defaults in medical imag ($Clip\ Limit \approx 2.0$, $Tile\ Size = 8 \times 8$), allowing both conservative and aggressive enhancement while avoiding noise amplification [15]. The objective was to maximize the SC. After optimization, the enhanced L channel was recombined with the a/b channels and converted back to RGB. One hundred images were selected via stratified random sampling (twenty images per class). The experiments were conducted on a system with Windows 11, an AMD Ryzen 5500 CPU, an Nvidia RTX 3060 12 GB GPU, 32 GB of RAM, and Python 3.11/OpenCV 4.9 (random seed=42). The performance was assessed through qualitative visual inspection by an anatomical pathologist, statistical analysis, and quantitative metrics: entropy, SSIM, PSNR, EME, RMSC, STD-DEV, and time process. A sensitivity analysis was conducted. Results indicated that minimal clip limits resulted in low-contrast images, while extremely high values increased noise and artifacts. Similarly, small tile grid sizes caused local over-enhancement, whereas huge grid sizes reduced local contrast. In addition, MobileNetV3-S was employed to evaluate Pap smear images enhanced through different optimization approaches (manual setting, FPA, and POA). The pretrained MobileNetV3-S model from TorchVision was utilized to classify the optimized SIPaKMeD images, thereby assessing the impact of contrast enhancement on downstream classification performance. The model was trained using the Adamax optimizer with a learning rate of 0.001 over 30 epochs, with the dataset split into 70% for training, 15% for validation, and 15% for testing.

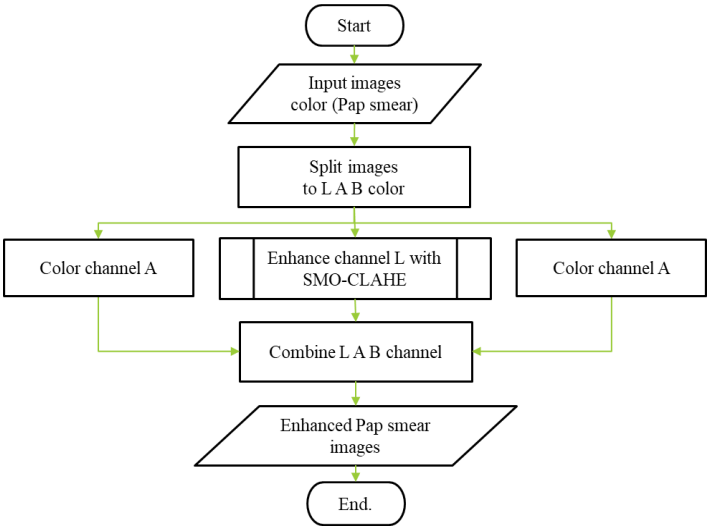

Figure 2. Simulation flowchart for SMO-CLAHE

2.6. Objective function (signal contrast)

In this study, we define SC as a combined measure of perceptual enhancement and fidelity. Let I_{orig} be the original image and I_{enh}. The CLAHE-enhanced image. We compute CEIQ(I_{enh}) and PSNR (I_{enh}, I_{orig}) (in dB). Because PSNR is expressed in decibels, we first normalize both metrics to the unit interval:

$$\widetilde{CEIQ} = \frac{CEIQ - CEIQ_{min}}{CEIQ_{max} - CEIQ_{min}}, \widetilde{PSNR} = \frac{PSNR - PSNR_{min}}{PSNR_{max} - PSNR_{min}} \quad (17)$$

The SC objective is then defined as the geometric mean (18):

$$SC = \sqrt{\widetilde{CEIQ} \times \widetilde{PSNR}} \quad (18)$$

We maximize SC with respect to CLAHE parameters (clip limit $\in$ [0.01,3.0], tile grid size $\in$ {2,…,16}). Normalization bounds (min/max) are computed from the current dataset range. This choice balances contrast enhancement (CEIQ) and noise suppression (PSNR) and avoids unit mismatch.

3. RESULTS AND DISCUSSION

This section presents the results of the SMO-CLAHE method through both visual inspection and quantitative analysis. A pathology specialist evaluated the images for clarity, contrast, and preservation of cellular structures across different enhancement techniques. For the quantitative assessment, various metrics were used, including entropy, EME, RMSC, STD-DEV, and CEIQ. The performance of the proposed method was compared to other optimization techniques, and statistical significance was assessed using a paired t-test. This statistical analysis helps confirm the improvements brought by the SMO-CLAHE method in terms of image quality and structural preservation.

3.1. Qualitative visual inspection

Pap-smear image analysis primarily focuses on accurately visualizing the nucleus and cytoplasm, as these structures are key to recognizing abnormal cell shapes and features, such as changes in nuclear size and shape, chromatin patterns, and the nucleus–to–cytoplasm (N/C) ratio [36]. To ensure clinical interpretability, the qualitative review by a specialist in anatomical pathology followed cytology-oriented quality criteria: i) nuclear contours are delineated with discernible chromatin texture; ii) cytoplasm is distinctly identifiable and uniformly visible, with intact boundaries and textural cues (vacuolation, perinuclear halo) preserved; iii) boundaries between nucleus–cytoplasm–background are well separated, minimizing artifacts such as haloing, ringing, blockiness, or stain-amplified speckle; iv) background cleanliness is adequate (suppression of debris and stain precipitates without erasing low-contrast actual structures); and v) in partially overlapping or crowded cells, intercellular interfaces remain discernible to support reliable estimation of nuclear size and N/C ratio [37]. These criteria directly reflect what cytologists require to judge pleomorphism, membrane irregularity, nucleolar prominence, and cytoplasmic changes during routine screening.

Figure 3 contrasts enhancement strategies on a SIPaKMeD sample. The original image (Figure 3(a)) exhibits low contrast and soft edges, obscuring nuclear rims and fine chromatin granules. The cytoplasmic boundaries blend with the background, and subtle perinuclear clearing is not reliably discernible. With Qassim's manual CLAHE (Figure 3(b)), global contrast and edge sharpness improve modestly; however, subtle nuclear texture and thin cytoplasmic margins remain partially veiled, and boundary transitions are not consistently crisp. FPA-optimized CLAHE (Figure 3(c)) sharpens nuclear rims and reveals more chromatin detail, better meeting the criteria than manual tuning, though localized haloing appears at some high-contrast interfaces. POA-optimized CLAHE (Figure 3(d)) further strengthens local contrast and boundary separation, improving differentiation of nucleus from cytoplasm in crowded fields; minor over-enhancement at peripheral cytoplasm may occur but generally remains controlled. The proposed SMO-CLAHE (Figure 3(e)) provides the most balanced outcome: nuclear edges are crisp, chromatin granularity is visible without clipping, cytoplasm is uniformly rendered with preserved texture, and interfaces with background are cleanly separated while artifacts (halo/ringing) are minimized. This balance is crucial: over-enhancement can create false edges or saturate chromatin, whereas under-enhancement can conceal diagnostically relevant details.

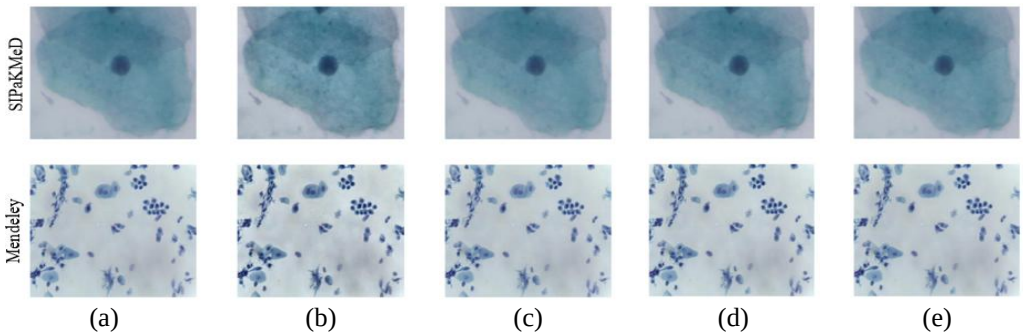

Figure 3. Comparative enhancement results on SIPaKMeD and Mendeley Pap smear dataset; (a) original, (b) Qassim manual setting CLAHE, (c) FPA-CLAHE, (d) POA-CLAHE, and (e) SMO-CLAHE

3.2. Statistical analysis

The paired t-test results provide strong evidence of SMO's effectiveness compared to manual and FPA, while showing comparable performance to POA in most metrics. For entropy, SMO does not differ significantly from POA (SIPaKMeD: $p=0.588$; Mendeley LBC: $p=1.0$), indicating both methods maintain information content at similar levels. However, significant differences against manual and FPA ($p<0.001$)

demonstrate SMO's ability to enhance entropy more effectively. Similarly, for SSIM, SMO achieves substantially higher values than manual and FPA across both datasets ($p<0.001$), confirming superior structural preservation, while remaining statistically indistinguishable from POA ($p>0.3$). PSNR results reinforce this trend: SMO is equivalent to POA ($p>0.09$) but significantly outperforms manual and FPA ($p<0.001$), which highlights its robustness in suppressing noise and reducing distortion. In contrast-related metrics (EME, RMSC, and STD-DEV), SMO and POA exhibit no significant differences ($p=1.0$), yet SMO consistently outperforms manual and FPA ($p<0.001$), underscoring its capacity for balanced contrast enhancement. The CEIQ metric further confirms these findings: SMO is comparable to POA but significantly superior to manual and FPA ($p<0.001$), reflecting its overall advantage in enhancing perceptual image quality.

Analysis of the fitness function also reveals SMO's superiority over manual and FPA ($p<0.001$), while maintaining parity with POA ($p>0.09$). Importantly, processing time results highlight SMO's efficiency, showing significantly faster execution than manual and FPA ($p<0.001$). Although differences with POA are dataset-dependent—non-significant for SIPaKMeD ($p=0.0879$) but significant for Mendeley ($p=7.79E-05$)—SMO generally maintains competitive runtime performance. These findings suggest that while POA and SMO achieve comparable outcomes in most image quality metrics, SMO demonstrates a clear and consistent advantage over manual and FPA methods. The results emphasize SMO's strength in balancing structural fidelity, contrast enhancement, and computational efficiency, making it a robust and reliable optimization strategy for Pap smear image enhancement. From a practical perspective, this implies that SMO can be adopted in real-world diagnostic workflows where high-quality images are critical for accurate classification, offering both quality improvement and reduced processing time compared to traditional and less advanced optimization approaches.

Figure 4 compares the relationship between processing time (Runtime) and reconstruction quality (PSNR) for four optimization methods across the SIPaKMeD see Figure 4(a) and Mendeley LBC see Figure 4(b) datasets. Each point represents a single optimized image. A desirable solution is located toward the upper-left corner, where PSNR is high and runtime is low. On both datasets, the manual settings form a tight cluster near the origin, indicating very short runtimes but consistently low PSNR. This confirms that manually chosen parameters cannot match the quality achieved by the automated optimizers. The FPA method displays a broad vertical spread of PSNR values but maintains relatively moderate runtimes (around 7–10 seconds). This suggests that FPA can occasionally reach higher PSNR, but its results are less stable and sometimes converge to sub-optimal quality. POA and SMO consistently achieve the highest PSNR values (approximately 45–50 dB) but require longer processing times (about 15–20 seconds). Between these two, SMO tends to form a slightly tighter cluster at the upper end of PSNR, indicating more reliable convergence to high-quality solutions. POA shows a slightly wider range of runtimes, reflecting more variability in computational cost. These results highlight a clear trade-off between image quality and computational effort. For practical applications, the choice of method should depend on operational constraints. In settings where high diagnostic accuracy is critical and computation time is less important, SMO is preferable. In time-sensitive clinical environments, FPA could be considered when a small loss in PSNR is acceptable to achieve faster turnaround.

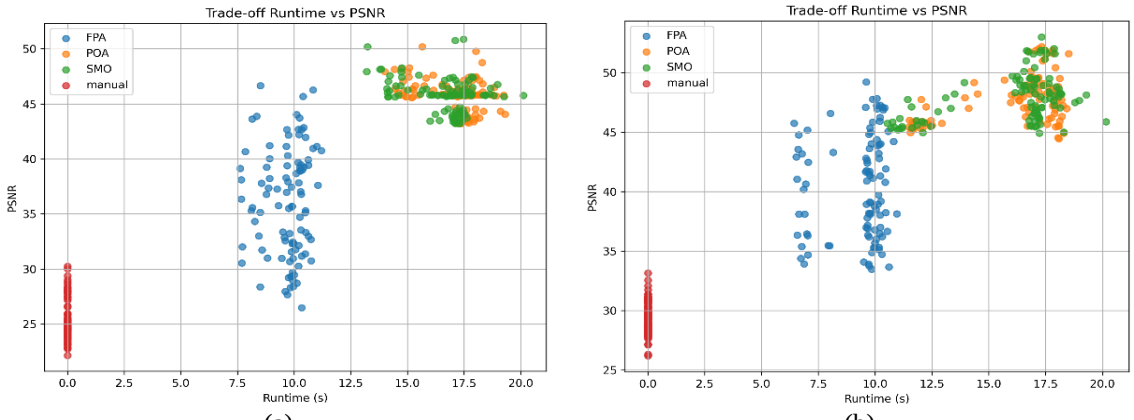

(a) (b)

Figure 4. Trade-off runtime vs PSNR; (a) SIPaKMeD and (b) Mendeley LBC dataset

3.3. Quantitative evaluation

The quantitative results presented in Tables 1 and 2 provide insights into the comparative performance of different optimization strategies—POA, FPA, SMO, and manual CLAHE parameter

settings—when applied to cervical cell image enhancement. Across both datasets, several consistent patterns can be observed in terms of entropy, SSIM, PSNR, local contrast measures (EME and RMSC), as well as perceptual quality indices (CEIQ and Finess), which together provide a comprehensive picture of image enhancement quality.

Table 1. Paired t-test on SIPaKMeD and Mendeley LBC datasets

	SipakMed dataset		Mendeley LBC dataset			
Metrics	SMO vs POA	SMO vs manual	SMO vs POA	SMO vs OA	SMO vs manual	SMO vs FPA
Entropy (t,p)	-5.44E+01	-1.54E+01	-6.23E+00	0.00E+00	-1.46E+01	-6.13E+00
	5.88E−01	4.59E−28	1.14E−08	1.00E+00	2.46E−26	1.79E−08
SSIM (t,p)	8.63E−01	4.12E+01	6.23E+00	1.00E+00	3.57E+01	6.42E+00
	3.90E−01	3.71E−64	1.17E−08	3.20E−01	2.60E−58	4.64E−09
PSNR (t,p)	8.30E−01	7.97E+01	1.67E+01	1.70E+00	1.19E+02	1.99E+01
	4.09E−01	1.33E−91	1.39E−30	9.30E−02	1.68E+08	2.68E−36
EME (t,p)	1.51E+00	-3.67E+01	-9.29E+00	0.00E+00	-4.10E+01	-1.03E+01
	1.34E−01	1.82E−59	3.85E−15	1.00E+00	6.48E−64	2.18E−17
RM SC (t,p)	-2.77E−01	-1.40E+01	-6.92E+00	0.00E+00	-2.84E+01	-1.14E+01
	7.83E−01	2.93E−25	4.60E−10	1.00E+00	2.04E−49	1.13E−19
STD-DEV	-5.26E−01	-1.28E+01	-5.98E+00	0.00E+00	-2.85E+01	-1.12E+01
(t,p)	6.00E−01	8.66E−23	3.60E−08	1.00E+00	1.52E−49	2.42E−19
CEIQ (t,p)	1.18E+00	-1.50E+01	-6.42E+00	0.00E+00	-2.06E+01	-6.58E+00
	2.40E−01	2.47E−27	4.84E−09	1.00E+00	1.24E−37	2.22E−09
Fitnes (t,p)	9.39E−01	5.84E+01	1.62E+01	1.70E+00	6.00E+01	1.97E+01
	3.50E−01	1.51E−78	1.37E−29	9.16E−02	1.11E−79	3.48E−36
Time (t,p)	-1.72E+00	6.57E+01	5.58E+01	-4.12E+00	1.19E+02	7.54E+01
	8.79E−02	1.77E−83	1.37E−76	7.97E−05	9.44E−109	2.78E−89

Table 2. Mean ± SD over 100 images for the metrics evaluation score on the SIPaKMeD dataset

Method	Entropy	SSIM	PSNR	EME	RMSC	STD_DEV	CEIQ	Fitness	Time (s)
POA	5.4688	0.9949	47.8379	0.8993	28.0784	36.0646	3.4517	0.6598	16.2019
FPA	5.5025	0.9880	40.3875	0.9931	28.6075	36.4409	3.4786	0.5464	**9.3081**
SMO	5.4686	**0.9950**	**47.9696**	0.9027	**28.0176**	36.0632	**3.5323**	**0.6621**	16.0380
Manual	**5.6389**	0.9427	29.4642	**1.3255**	30.3599	**37.7466**	3.4644	0.2828	-

On SIPaKMeD, both SMO and POA achieved nearly identical outcomes in most metrics, with SMO showing a slight edge in PSNR (47.97 vs. 47.83) and CEIQ (3.53 vs. 3.45). This suggests that SMO was more effective in preserving image quality while improving perceptual contrast. FPA, although competitive in entropy (5.50) and RMS contrast (28.60), exhibited a notably lower SSIM (0.9880) and PSNR (40.38), indicating that images enhanced by FPA suffered some structural distortions and reduced noise suppression compared to SMO and POA. The manual CLAHE setting, while producing the highest entropy (5.64) and RMS contrast (30.36), demonstrated a clear decline in SSIM (0.9427) and PSNR (29.46). These results indicate that manual parameter tuning tends to over-amplify contrast at the cost of image fidelity, introducing excessive noise and structural distortions. Furthermore, the Finess score for the manual method (60.5464) was substantially lower than that of SMO and POA (>6590), reflecting weaker enhancement consistency. In terms of processing time, FPA consistently required the least computational cost (9.31 s), while SMO and POA were more time-intensive (~16 s). This trade-off highlights that while FPA is efficient, its reduction in image fidelity makes SMO and POA more suitable choices for medical image preprocessing.

The results on the Mendeley dataset reaffirmed the trends observed in SIPaKMeD, as shown in Table 3. SMO and POA again achieved the highest PSNR values (45.84 and 45.79, respectively) with superior SSIM (~0.9968), indicating strong preservation of structural content. Notably, SMO consistently produced a higher CEIQ score (3.55) compared to POA (3.45). It means that its optimization strategy better balances enhancement and perceptual quality. FPA yielded higher entropy (5.29) and RMS contrast (28.53) than SMO/POA, but at the expense of PSNR (36.01), implying suboptimal suppression of noise artifacts. Manual settings once again produced the highest entropy (5.50) and RMS contrast (33.18). Still, these gains came with severe degradation in PSNR (25.26) and SSIM (0.9360), underscoring the risks of heuristic parameter tuning in sensitive medical imagery. The Finess scores followed a similar pattern to SIPaKMeD, with SMO and POA (~0.6270) outperforming both FPA (0.4371) and manual (0.2761). This suggests that stochastic optimization approaches provide more stable and reliable enhancements across diverse image samples. In terms of time efficiency, FPA was again the fastest (~9.69 s), while SMO and POA required nearly double the processing time.

Table 3. Mean±SD over 100 images for the metrics evaluation score on the Mendeley LBC dataset

Method	Entropy	SSIM	PSNR	EME	RMSC	std_dev	CEIQ	Fitness	Time (s)
POA	5.2068	0.9967	45.7861	3.1804	**26.7959**	28.3258	3.4463	0.6271	17.0684
FPA	5.2856	0.9904	36.0117	3.4147	28.5303	29.9441	3.4845	0.4371	**9.6942**
SMO	5.2068	**0.9968**	**45.8372**	3.1804	**26.7959**	28.3258	**3.5463**	**0.6280**	16.6525
Manual	**5.5001**	0.9360	25.2623	**4.1819**	33.1796	**34.3198**	3.4840	0.2761	-

Comparing both datasets, it is evident that SMO maintained the most consistent performance across evaluation metrics, with the highest CEIQ scores (3.53 on SIPaKMeD and 3.55 on Mendeley) and competitive PSNR and SSIM values. POA showed nearly identical results but slightly lagged in CEIQ, suggesting that SMO's swarm-based adaptive search provides an edge in balancing structural fidelity and perceptual quality. The manual method consistently amplified entropy and RMS contrast but suffered from poor structural similarity and perceptual quality indices, confirming that manual tuning risks over-enhancement. Meanwhile, FPA demonstrated strengths in efficiency but compromised structural integrity, making it less suitable for medical preprocessing tasks where diagnostic accuracy depends on image fidelity.

3.4. Image classification performance

The evaluation of MobileNetV3-S on the SIPaKMeD dataset reveals that contrast enhancement using CLAHE significantly improves classification performance, as shown in Figure 5. For the original image, the model achieved an accuracy of 90.57% with balanced precision and recall, confirming that MobileNetV3-S is effective at extracting features from cytological images. However, applying CLAHE with manually selected parameters improved all metrics, increasing accuracy to 92.82% and the F1-score to 92.61%. This suggests that enhancing local contrast helps the model capture more distinctive cellular structures. Further gains were made through metaheuristic-based optimization of CLAHE parameters. The FPA achieved an accuracy of 93.12%, with a precision of 94.37% and a recall of 93.65%, effectively balancing false positives and false negatives. The POA achieved a slightly higher accuracy of 93.22%. However, its recall of 93.16% was marginally lower than FPA's, indicating POA provided good overall enhancement but was less effective at identifying all abnormal cases. The best results were achieved by the SMO, which attained the highest accuracy of 93.47%, with precision and recall at 94.46% and 94.18%, respectively. This demonstrates that SMO is particularly effective in optimizing CLAHE parameters, resulting in improved feature visibility and more reliable classification. Although the F1-score under SMO (92.94%) was similar to POA's, the improved recall is significant in medical diagnostics, as it reduces the chance of missing precancerous or malignant cells. The SMO-CLAHE method offers a robust and efficient framework for cervical cancer classification, achieving high accuracy while remaining computationally lightweight enough for use in clinical or resource-limited settings.

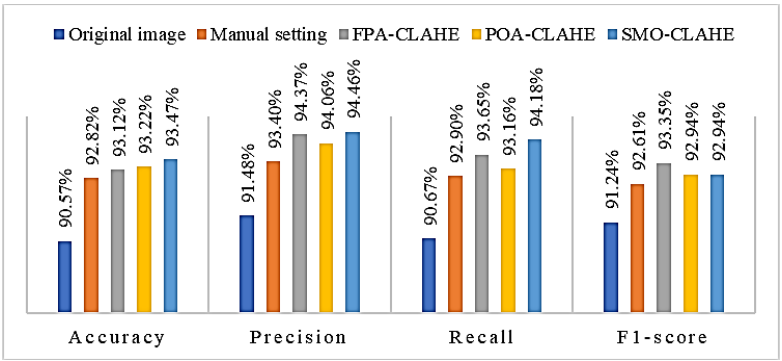

Figure 5. MobileNetV3-S performance over optimized SIPaKMeD images dataset

4. CONCLUSION

This study presented SMO-CLAHE, an image enhancement framework that leverages SMO with a SC objective to adaptively optimize CLAHE parameters. The proposed approach successfully balances contrast enhancement with noise suppression, as validated on SIPaKMeD and Mendeley datasets. Compared with manual CLAHE and FPA, SMO-CLAHE delivered significant improvements across multiple metrics, while maintaining comparable performance to POA. Crucially, downstream classification with MobileNetV3-S confirmed that enhanced images not only improve visual clarity but also strengthen diagnostic accuracy. The findings establish SMO-CLAHE as a reliable and efficient preprocessing technique

for cervical cytology, suitable for integration into clinical image analysis workflows. Looking forward, future research should: i) investigate parameter sensitivity and optimization stability across diverse imaging conditions, ii) broaden expert-based qualitative evaluation for clinical adoption, iii) validate performance on additional Pap smear and histopathological datasets, and iv) explore integration with deep learning segmentation and classification pipelines. These directions will further enhance the generalizability and clinical impact of SMO-CLAHE, advancing the development of automated and reliable cervical cancer detection systems.

FUNDING INFORMATION

This research received financial support from the Ministry of Higher Education, Science, and Technology of the Republic of Indonesia in partnership with the Indonesian Endowment Fund for Education (LPDP). The funding was granted through the Indonesian Education Scholarship (BPI) program, administered by the Center for Higher Education Funding and Assessment (PPAPT). BPI ID: 202327091034.

AUTHOR CONTRIBUTIONS STATEMENT

This journal uses the Contributor Roles Taxonomy (CRediT) to recognize individual author contributions, reduce authorship disputes, and facilitate collaboration.

Name of Author	C	M	So	Va	Fo	I	R	D	O	E	Vi	Su	P	Fu
Ach Khozaimi	✓	✓	✓		✓	✓			✓		✓		✓	✓
Wuryansari Muharini Kusumawinahyu		✓		✓	✓		✓			✓		✓		
Isnani Darti	✓	✓	✓			✓	✓	✓		✓		✓		
Syaiful Anam	✓	✓		✓						✓		✓	✓	
Ulfatun Nahdhiyah		✓		✓	✓					✓	✓			

C : **C**onceptualization
M : **M**ethodology
So : **So**ftware
Va : **Va**lidation
Fo : **Fo**rmal analysis
I : **I**nvestigation
R : **R**esources
D : **D**ata Curation
O : Writing - **O**riginal Draft
E : Writing - Review & **E**diting
Vi : **Vi**sualization
Su : **Su**pervision
P : **P**roject administration
Fu : **Fu**nding acquisition

CONFLICT OF INTEREST STATEMENT

The authors declare no conflicts of interest or relationships that could influence this work.

DATA AVAILABILITY

This study used the SIPaKMeD and Mendeley datasets, available at https://bit.ly/SIPaKMeD and https://data.mendeley.com/datasets/zddtpgzv63/4.

REFERENCES

[1] D. Viveros-Carreño, A. Fernandes, and R. Pareja, "Updates on cervical cancer prevention," *International Journal of Gynecological Cancer*, vol. 33, no. 3, pp. 394–402, Mar. 2023, doi: 10.1136/ijgc-2022-003703.
[2] D. Sambyal and A. Sarwar, "Recent developments in cervical cancer diagnosis using deep learning on whole slide images: An Overview of models, techniques, challenges and future directions," *Micron*, vol. 173, p. 103520, Oct. 2023, doi: 10.1016/j.micron.2023.103520.
[3] A. Khozaimi and W. F. Mahmudy, "New insight in cervical cancer diagnosis using convolution neural network architecture," *IAES International Journal of Artificial Intelligence (IJ-AI)*, vol. 13, no. 3, pp. 3092–3100, Sep. 2024, doi: 10.11591/ijai.v13.i3.pp3092-3100.
[4] K. P. Win, Y. Kitjaidure, K. Hamamoto, and T. M. Aung, "Computer-assisted screening for cervical cancer using digital image processing of pap smear images," *Applied Sciences*, vol. 10, no. 5, pp. 1–22, Mar. 2020, doi: 10.3390/app10051800.
[5] E. A. Tjoa, I. P. Y. N. Suparta, R. Magdalena, and N. K. CP, "The use of CLAHE for improving an accuracy of CNN architecture for detecting pneumonia," *SHS Web of Conferences*, vol. 139, p. 03026, May 2022, doi: 10.1051/shsconf/202213903026.
[6] J. Guo, J. Ma, Á. F. García-Fernández, Y. Zhang, and H. Liang, "A survey on image enhancement for Low-light images," *Heliyon*, vol. 9, no. 4, pp. 1–26, Apr. 2023, doi: 10.1016/j.heliyon.2023.e14558.
[7] I. M. Mohammed and N. A. M. Isa, "Contrast Limited Adaptive Local Histogram Equalization Method for Poor Contrast Image Enhancement," *IEEE Access*, vol. 13, pp. 62600–62632, 2025, doi: 10.1109/ACCESS.2025.3558506.
[8] A. Desiani, M. Erwin, B. Suprihatin, S. Yahdin, A. I. Putri, and F. R. Husein, "Bi-path Architecture of CNN Segmentation and

Classification Method for Cervical Cancer Disorders Based on Pap-smear Images," *IAENG International Journal of Computer Science*, vol. 48, no. 3, pp. 1–9, 2021.
[9] R. C. Chen, C. Dewi, Y. C. Zhuang, and J. K. Chen, "Contrast Limited Adaptive Histogram Equalization for Recognizing Road Marking at Night Based on Yolo Models," *IEEE Access*, vol. 11, pp. 92926–92942, 2023, doi: 10.1109/ACCESS.2023.3309410.
[10] M. Hayati *et al.*, "Impact of CLAHE-based image enhancement for diabetic retinopathy classification through deep learning," *Procedia Computer Science*, vol. 216, pp. 57–66, 2022, doi: 10.1016/j.procs.2022.12.111.
[11] S. Saifullah and R. Drezewski, "Modified Histogram Equalization for Improved CNN Medical Image Segmentation," *Procedia Computer Science*, vol. 225, pp. 3021–3030, 2023, doi: 10.1016/j.procs.2023.10.295.
[12] S. Asghar *et al.*, "Water Classification Using Convolutional Neural Network," *IEEE Access*, vol. 11, pp. 78601–78612, 2023, doi: 10.1109/ACCESS.2023.3298061.
[13] H. M. Qassim, N. M. Basheer, and M. N. Farhan, "Brightness preserving enhancement for dental digital x-ray images based on entropy and histogram analysis," *Journal of Applied Science and Engineering*, vol. 22, no. 1, pp. 187–194, 2019, doi: 10.6180/jase.201903_22(1).0019.
[14] L. G. More, M. A. Brizuela, H. L. Ayala, D. P. Pinto-Roa, and J. L. V. Noguera, "Parameter tuning of CLAHE based on multi-objective optimization to achieve different contrast levels in medical images," in *2015 IEEE International Conference on Image Processing (ICIP)*, Quebec City, QC, Canada, IEEE, Sep. 2015, pp. 4644–4648, doi: 10.1109/ICIP.2015.7351687.
[15] A. Fawzi, A. Achuthan, and B. Belaton, "Adaptive Clip Limit Tile Size Histogram Equalization for Non-Homogenized Intensity Images," *IEEE Access*, vol. 9, pp. 164466–164492, 2021, doi: 10.1109/ACCESS.2021.3134170.
[16] U. Kuran and E. C. Kuran, "Parameter selection for CLAHE using multi-objective cuckoo search algorithm for image contrast enhancement," *Intelligent Systems with Applications*, vol. 12, pp. 1–13, Nov. 2021, doi: 10.1016/j.iswa.2021.200051.
[17] U. Kuran, E. C. Kuran, and M. B. Er, "Parameter Selection of Contrast Limited Adaptive Histogram Equalization Using Multi-Objective Flower Pollination Algorithm," in *International Congress of Electrical and Computer Engineering*, Cham: Springer International Publishing, 2022, vol. 436, pp. 109–123, doi: 10.1007/978-3-031-01984-5_9.
[18] S. Surya and A. Muthukumaravel, "Adaptive Sailfish Optimization-Contrast Limited Adaptive Histogram Equalization (ASFO-CLAHE) for Hyperparameter Tuning in Image Enhancement," in *Computational Intelligence for Clinical Diagnosis*, vol. Part F274, S. I. Publishing, Ed., 2023, pp. 57–76, doi: 10.1007/978-3-031-23683-9_5.
[19] S. R. Borra, N. P. Tejaswini, V. Malathy, B. M. Kumar, and M. I. Habelalmateen, "Contrast Limited Adaptive Histogram Equalization based Multi-Objective Improved Cat Swarm Optimization for Image Contrast Enhancement," in *2023 International Conference on Integrated Intelligence and Communication Systems (ICIICS)*, Kalaburagi, India, IEEE, Nov. 2023, pp. 1–5, doi: 10.1109/ICIICS59993.2023.10420959.
[20] Y. R. Haddadi, B. Mansouri, and F. Z. I. Khodja, "A novel medical image enhancement algorithm based on CLAHE and pelican optimization," *Multimedia Tools and Applications*, vol. 83, no. 42, pp. 90069–90088, Apr. 2024, doi: 10.1007/s11042-024-19070-6.
[21] W. Sultana and S. D. S. Jebaseelan, "Optimal allocation of solar PV and wind energy power for radial distribution system using spider monkey optimization," *Sustainable Computing: Informatics and Systems*, vol. 42, p. 100986, Apr. 2024, doi: 10.1016/j.suscom.2024.100986.
[22] H. Zhu, Y. Wang, Z. Ma, and X. Li, "A comparative study of swarm intelligence algorithms for UCAV path-planning problems," *Mathematics*, vol. 9, no. 2, pp. 1–31, Jan. 2021, doi: 10.3390/math9020171.
[23] C. Hu, H. Li, T. Ma, C. Zeng, and X. Ji, "An improved image enhancement algorithm: Radial contrast-limited adaptive histogram equalization," *Multimedia Tools and Applications*, vol. 83, no. 36, pp. 83695–83707, Mar. 2024, doi: 10.1007/s11042-024-18922-5.
[24] J. Yan, J. Li, and X. Fu, "No-Reference Quality Assessment of Contrast-Distorted Images using Contrast Enhancement," *arXiv preprint*, pp. 1–15, 2019, doi: 10.48550/arXiv.1904.08879.
[25] R. Kumar and A. K. Bhandari, "Noise reduction deep CNN-based retinal fundus image enhancement using recursive histogram," *Neural Computing and Applications*, vol. 36, no. 27, pp. 17221–17243, Sep. 2024, doi: 10.1007/s00521-024-09996-1.
[26] Y. Qi *et al.*, "A Comprehensive Overview of Image Enhancement Techniques," *Archives of Computational Methods in Engineering*, vol. 29, no. 1, pp. 583–607, Jan. 2022, doi: 10.1007/s11831-021-09587-6.
[27] S. M. Pizer *et al.*, "Adaptive Histogram Equalization and Its Variations," *Computer vision, graphics, and image processing*, vol. 39, no. 3, pp. 355–368, Sep. 1987, doi: 10.1016/S0734-189X(87)80186-X.
[28] K. G. Dhal, A. Das, S. Ray, J. Gálvez, and S. Das, "Histogram Equalization Variants as Optimization Problems: A Review," *Archives of Computational Methods in Engineering*, vol. 28, no. 3, pp. 1471–1496, May. 2021, doi: 10.1007/s11831-020-09425-1.
[29] Y. Yoshimi *et al.*, "Image preprocessing with contrast-limited adaptive histogram equalization improves the segmentation performance of deep learning for the articular disk of the temporomandibular joint on magnetic resonance images," *Oral Surgery, Oral Medicine, Oral Pathology and Oral Radiology*, vol. 138, no. 1, pp. 128–141, Jul. 2024, doi: 10.1016/j.oooo.2023.01.016.
[30] E. Sandhya and A. Kumarappan, "Enhancing the Performance of an Intrusion Detection System Using Spider Monkey Optimization in IoT," *International Journal of Intelligent Engineering and Systems*, vol. 14, no. 6, pp. 30–39, 2021, doi: 10.22266/ijies2021.1231.04.
[31] A. Agrawal, D. Garg, R. Sethi, and A. K. Shrivastava, "Optimum redundancy allocation using spider monkey optimization," *Soft Computing*, vol. 27, no. 21, pp. 15595–15608, Nov. 2023, doi: 10.1007/s00500-023-08746-0.
[32] V. Kamble and K. M. Bhurchandi, "No-reference image quality assessment algorithms: A survey," *Optik*, vol. 126, no. 11–12, pp. 1090–1097, Jun. 2015, doi: 10.1016/j.ijleo.2015.02.093.
[33] C. Avatavului and M. Prodan, "Evaluating Image Contrast: A Comprehensive Review and Comparison of Metrics," *Journal of Information Systems & Operations Management*, vol. 17, no. 1, pp. 143–160, 2023.
[34] M. E. Plissiti, P. Dimitrakopoulos, G. Sfikas, C. Nikou, O. Krikoni, and A. Charchanti, "Sipakmed: A New Dataset for Feature and Image Based Classification of Normal and Pathological Cervical Cells in Pap Smear Images," in *2018 25th IEEE International Conference on Image Processing (ICIP)*, Athens, Greece: IEEE, Oct. 2018, pp. 3144–3148, doi: 10.1109/ICIP.2018.8451588.
[35] P. R. Narkhede and A. V. Gokhale, "Color image segmentation using edge detection and seeded region growing approach for CIELab and HSV color spaces," in *2015 International Conference on Industrial Instrumentation and Control, ICIC 2015*, Pune, India: IEEE, May. 2015, pp. 1214–1218, doi: 10.1109/IIC.2015.7150932.
[36] S. Ahlawat *et al.*, "Cytopathology Using High Resolution Digital Holographic Microscopy," in *Augmented Reality and Its Application*, IntechOpen, 2022, doi: 10.5772/intechopen.96459.
[37] M. A. Pangarkar, "The Bethesda System for reporting cervical cytology," *CytoJournal*, vol. 19, p. 28, Apr. 2022, doi: 10.25259/CMAS_03_07_2021.

BIOGRAPHIES OF AUTHORS

Ach Khozaimi is a lecturer in Informatics Engineering at Trunojoyo University of Madura, Indonesia. He earned his bachelor's degree in Informatics from Trunojoyo University of Madura and his master's degree in Informatics from Institut Teknologi Sepuluh Nopember (ITS), Indonesia. Currently, he is pursuing a Ph.D. in the Mathematics Department at Brawijaya University, Indonesia. His doctoral studies are funded by the Center for Higher Education Funding and Assessment (PPAPT) under the Ministry of Higher Education, Science, and Technology of the Republic of Indonesia. He can be contacted at email: khozaimi@trunojoyo.ac.id.

Wuryansari Muharini Kusumawinahyu received her Doctoral Degree in Mathematics from Institut Teknologi Bandung (ITB), Indonesia in 2006. She also earned her Bachelor's Degree in Mathematics from ITB in 1991 and her Master's Degree from the same institution in 1995. She is currently an associate professor at the Department of Mathematics, Faculty of Mathematics and Natural Sciences (FMIPA), Universitas Brawijaya, Malang, Indonesia. Her research includes mathematical epidemiology, predator-prey models, and wave dynamics. She has published numerous papers in national and international journals. She can be contacted at email: wmuharini@ub.ac.id.

Dr. Isnani Darti stands as the 24th active Professor at the Faculty of Mathematics and Natural Sciences (FMIPA). Her research interests span several captivating domains: applied dynamical systems, mathematical biology, optical solitons, and discretization of continuous dynamical systems. Recently, she achieved the prestigious rank of Professor at Brawijaya University. She is the 24th active Professor at the Faculty of Mathematics and Natural Sciences (FMIPA) and the 176th active at the university overall. Her professorship adds to the rich legacy of Brawijaya University, where she is the 335th Professor in its history. She can be contacted at email: isnanidarti@ub.ac.id.

Syaiful Anam received a Doctor of Natural Science and Mathematics degree from Yamaguchi University, Japan in 2015. He also received his Bachelor's Degree in Mathematics from Brawijaya University, Indonesia in 2001 and his Master Degree from Sepuluh Nopember Institute of Technology, Indonesia in 2006. He is currently an associate professor at Mathematics Department, Brawijaya University, Malang, Indonesia. His research includes data science, computational intelligence, machine learning, digital image processing, and computer vision. He has published over 35 papers in international journals and conferences. He can be contacted at email: syaiful@ub.ac.id.

Ulfatun Nahdhiyah earned her medical degree from the Faculty of Medicine, Universitas Islam Malang, Indonesia, in 2015. She is currently pursuing a specialist degree in Anatomical Pathology at Universitas Brawijaya, Malang, Indonesia, which she commenced in February 2023. Her research interests focus on cervical cancer, particularly in diagnostic pathology and histopathological analysis. She can be contacted at email: ufa.nahdhiyah@gmail.com.